6 Neutrino Oscillations and CKM Measurements

The quark and lepton mass eigenstates result from the diagonalization of the Higgs-fermion Yukawa couplings between the three mass generations of $SU(2)_L$ doublets and right-handed singlets. The gauge interactions, on the other hand, connect only left-to-left- and right-to-right-handed chirality fermion components. Therefore, gauge interactions that are diagonal in flavor will be unaffected by the phases associated with the unitary rotations for mass diagonalization, as $(U_R^u)^\dagger U_R^u = (U_R^d)^\dagger U_R^d = 1$ and $(U_L^u)^\dagger U_L^u = (U_L^d)^\dagger U_L^d = 1$. However, the charged-current interaction is affected by these rotations, resulting in two separate mixing matrices for quarks and leptons,

$$V_{UD} = U_L^u (U_L^d)^\dagger, \qquad V' = U_L^\nu (U_L^\ell)^\dagger, \tag{6.1}$$

where U_L^u and U_L^d are 3×3 matrices for up-type and down-type left-handed chirality quarks, respectively, and similarly, U_L^ν and U_L^ℓ are 3×3 matrices for neutral and charged left-handed chirality leptons, respectively.

In the case of the quark sector, the u-quark is the only absolutely stable particle. The d-quark through baryon number conservation is stable if within the bound state of a proton. All other quarks decay through the charged-current interaction into the u-quark either directly or via cascade decays. With the exception of the top quark, the quarks interact via the flavor-diagonal QCD interaction on a time scale much shorter than their weak decays. Hence, the flavor of the quark is effectively projected out by the hadronic mass eigenstate that is formed shortly after quark production. The quark-mixing matrix elements act as vertex coefficients for setting the probability to project into a particular quark flavor. Once the quark is in a hadronic state, then the hadronic state may oscillate into other hadronic states if there are degeneracies or near degeneracies in the masses of hadrons and a transition amplitude that connects the states. In particular, hadronic states connected through a transition amplitude involving the weak charged current will be nearly degenerate due to the relative strength of the weak interaction. This is precisely the situation for neutral mesons whose particle and antiparticle states are separate, namely, the K^0–$\bar{K}^0$, D^0–$\bar{D}^0$, B_d^0–$\bar{B}_d^0$, and B_s^0–$\bar{B}_s^0$ systems.

The lepton sector on the other hand has four stable particles, the electron and the three neutrino families. The neutrinos do not interact rapidly after being produced and remain

insulated from Standard Model interactions over a long time scale. In addition, the neutrino masses are much more degenerate than the quark masses, so mass selection does not occur as rapidly. Therefore, the neutrino is not rapidly projected into a mass eigenstate following production, but rather is treated as being created in a pure flavor eigenstate tagged by the associated charged lepton in charged-current production. The neutrino then oscillates in flavor during free-particle propagation according to the squared mass differences between nearly degenerate neutrino mass eigenstates. Each mass eigenstate has a nondiagonal flavor composition. The neutrino flavor is then projected out after a finite propagation length through the flavor of the charged lepton created at detection time. Therefore, the natural choice of a mixing matrix in the lepton sector is not V' but rather $(U_L^{\nu})^{\dagger}$, which transforms the neutrino mass eigenstates $\nu = (\nu_1, \nu_2, \nu_3)$ into the neutrino flavor eigenstates $\nu' = (\nu_e, \nu_\mu, \nu_\tau)$, i.e., $\nu' = (U_L^{\nu})^{\dagger}\nu$. The exception to the vacuum oscillation description of the neutrino flavor mixing is in the case where the neutrino is produced in the center of the sun where coherent forward-scattering can occur and where energetic neutrinos will adiabatically fall into mass eigenstates before leaving the solar mass. This exception will be discussed in the section on solar neutrinos.

What is common to both quark and lepton sectors is that the mismatch between weak interaction states and mass eigenstates can give rise to the phenomenon of oscillations. Two types of systems are known to exhibit measurable oscillations: the neutrinos that mix in flavor and the neutral mesons that mix particle and antiparticle states.

6.1 Neutrino Oscillations

The existence of observable interference and oscillations in the propagation of the states requires an uncertainty in energy and momentum of the source of the particles, related to the localization in space and time of the particle production. A quantitative estimate can be taken from the energy uncertainty of neutrinos produced from charged pions decaying to muons. In the π^+ rest frame, the decay kinematics are

$$p_\mu^2 = m_\mu^2 = (p_\pi - p_\nu)^2 = m_\pi^2 + m_\nu^2 - 2p_\pi \cdot p_\nu = m_\pi^2 + m_\nu^2 - 2m_\pi E_\nu. \tag{6.2}$$

This gives

$$E_\nu = \frac{m_\pi^2 + m_\nu^2 - m_\mu^2}{2m_\pi}. \tag{6.3}$$

Therefore, if we consider two possible neutrino mass eigenstates ν_1 and ν_2, then the difference in the produced neutrino energy is related to the difference in the squared neutrino masses

$$E_{\nu_1} - E_{\nu_2} = \frac{m_{\nu_1}^2 - m_{\nu_2}^2}{2m_\pi}. \tag{6.4}$$

The π^+ width is $\Gamma_\pi \simeq 2.5 \cdot 10^{-8}$ eV, which can compared directly to the energy difference of the produced neutrinos $|E_{\nu_1} - E_{\nu_2}|$. Therefore, coherent oscillations will not be present in neutrino mass eigenstates from charged pion decay for squared mass differences greater than $\approx 7\ (\text{eV})^2$.

A neutrino produced in a charged-current decay is flavor tagged at creation according to the charged lepton type. The neutrino flavor eigenstates will be denoted as $|\nu_\alpha\rangle$ and the mass eigenstates as $|\nu_i\rangle$ with masses m_i. Therefore, at $t=0$ the state $|\nu_\alpha\rangle$ can be expanded in terms of $|\nu_i\rangle$

$$|\nu_\alpha\rangle = \sum_i U_{\alpha i}^* |\nu_i\rangle \tag{6.5}$$

where $U_{\alpha i}^*$ is known as the Maki-Nakagawa-Sakata (MNS) matrix (3.195). At finite t, the expression for the time evolution of a momentum eigenstate is given by

$$|\nu(t)\rangle = \sum_i U_{\alpha i}^* \exp(-iE_i t + i\mathbf{p}\cdot\mathbf{x})|\nu_i\rangle. \tag{6.6}$$

If at time t the neutrino state interacts weakly, the probability that this interaction results in a flavor tag $|\nu_\beta\rangle$ is

$$P(\nu_\alpha \to \nu_\beta) = |\langle\nu_\beta|\nu(t)\rangle|^2 = \left|\sum_i U_{\alpha i}^* U_{\beta i} \exp(-iE_i t)\right|^2. \tag{6.7}$$

In the ultrarelativistic limit, we can expand the energy-momentum relationship in the leading mass term

$$E_i = p + \frac{m_i^2}{2p} \tag{6.8}$$

so that

$$P(\nu_\alpha \to \nu_\beta) = |\langle\nu_\beta|\nu(t)\rangle|^2 = \left|\sum_i U_{\alpha i}^* U_{\beta i} \exp\left(-i\frac{m_i^2 t}{2p}\right)\right|^2 \tag{6.9}$$

for neutrinos propagating in vacuum. In the case of two generations, the one-parameter rotation matrix is given by

$$U = \begin{pmatrix} \cos\theta & \sin\theta \\ -\sin\theta & \cos\theta \end{pmatrix}. \tag{6.10}$$

For an electron-flavor initial state $\alpha = e$, we get the probability of $\nu_e \to \nu_\mu$ oscillation to be

$$\begin{aligned} P(\nu_e \to \nu_\mu) &= \left|U_{e1}^* U_{\mu 1} \exp\left(-i\frac{m_1^2 t}{2p}\right) + U_{e2}^* U_{\mu 2} \exp\left(-i\frac{m_2^2 t}{2p}\right)\right| \\ &= \left|-\cos\theta\sin\theta\exp\left(-i\frac{(m_1^2 - m_2^2)t}{2p}\right) + \sin\theta\cos\theta\right|^2 \\ &= 2\cos^2\theta\sin^2\theta \\ &\quad -\cos^2\theta\sin^2\theta\left(\exp\left(-i\frac{(m_1^2 - m_2^2)t}{2p}\right) + \exp\left(i\frac{(m_1^2 - m_2^2)t}{2p}\right)\right) \\ &= 2\cos^2\theta\sin^2\theta\left(1 - \cos\left(\frac{(m_1^2 - m_2^2)t}{2p}\right)\right) \\ &= \sin^2 2\theta \sin^2\left(\frac{1.27\Delta m^2 L}{E}\right) \end{aligned} \tag{6.11}$$

where in the last expression L is in m, E is in MeV, and Δm^2 is in eV^2, giving the resulting coefficient $(10^{-6})^2/(197\ \text{MeV fm})/4 = 1.27\ \text{MeV (eV)}^{-2}\ \text{m}^{-1}$. The general expression for a neutrino flavor oscillation for three mass generations $i(j) = 1, 2, 3\ (1, 2, 3)$ is given by

$$\begin{aligned} P(\nu_\alpha \to \nu_\beta) = \delta_{\alpha\beta} & \\ & -4\sum_{i>j} \mathcal{R}e\{U^*_{\alpha i} U_{\alpha j} U_{\beta i} U^*_{\beta j}\} \sin^2\left(\frac{1.27\Delta m^2_{ij} L}{E}\right) \\ & +2\sum_{i>j} \mathcal{I}m\{U^*_{\alpha i} U_{\alpha j} U_{\beta i} U^*_{\beta j}\} \sin\left(\frac{2(1.27)\Delta m^2_{ij} L}{E}\right) \end{aligned} \tag{6.12}$$

where $\Delta m^2_{ij} = m^2_i - m^2_j$. In equation (6.11), there are three important ranges of the argument $\Delta m^2 L/E$:

$$\begin{aligned} &\Delta m^2 L/E \ll 1 \quad \text{no oscillations, } P(\nu_e \to \nu_\mu) \approx 0, \\ &\Delta m^2 L/E \sim 1 \quad \theta \text{ and } |\Delta m^2| \text{ can be determined,} \\ &\Delta m^2 L/E \gg 1 \quad \text{rapid oscillations, } \bar{P}(\nu_e \to \nu_\mu) = \frac{1}{2}\sin^2 2\theta, \end{aligned} \tag{6.13}$$

where $\bar{P}$ is the time-integrated average oscillation probability.

6.1.1 Atmospheric and Accelerator-Based Neutrino Experiments

Atmospheric neutrinos come from the leptonic decays of mesons and heavy leptons produced in cosmic ray showers. When a high-energy proton impinges on the gaseous atmosphere of Earth, a multiplicity of pions can be produced when the proton scatters via the strong interaction with a nucleon in the atmosphere. The longitude and latitude of the proton impact point on Earth's atmosphere defines an approximate distance L between the location of the cosmic ray shower and the position of a neutrino detector located at some fixed position underground. Here, L will vary from on order 10–100 km for cosmic ray showers produced in the atmosphere directly above the detector to the diameter of Earth, or approximately 12,500–13,000 km for cosmic ray showers on the opposite side of the planet. Atmospheric neutrinos contain a mix of ν_μ and ν_e and their antiparticles from charged pion decay $\pi^\pm \to \mu^\pm + \nu_\mu(\bar{\nu}_\mu)$ and subsequent muon decay $\mu^\pm \to e^\pm + \nu_e(\bar{\nu}_e) + \bar{\nu}_\mu(\nu_\mu)$. Neutrinos passing through a detector will have a small but finite probability to scatter via the neutral- and charged-current weak interactions. The neutral-current weak interactions, Z-boson exchange, is lepton-flavor independent. The charged-current weak interaction will tag the flavor of the lepton with some flavor bias from processes involving atomic electrons in the scattering material. In the atmospheric data there is a clear depletion of ν_μ, whereas the ν_e flux appears constant as a function of propagation length L from the origin of the cosmic ray shower as determined from the angular information of the particles scattered by the interacting neutrino within the detector. The data from the SuperK experiment is shown in figure 6.1 as a function of L/E for electron-type and muon-type neutrino scattering events [1].

The peak of the cosmic muon neutrino energy spectrum is ~2 GeV, which, given Earth's diameter, is ideally suited for oscillation measurements for squared mass differences of

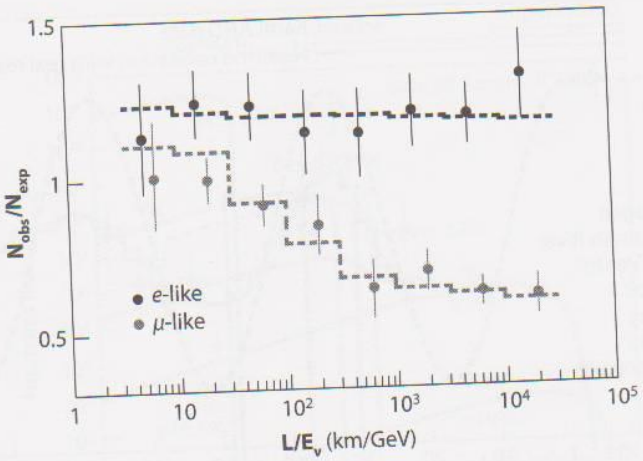

FIGURE 6.1. Observed flux of electron-type and muon-type scattering events from the Super-Kamiokande atmospheric neutrino data as a function of L/E and normalized to the expected flux from a Monte Carlo simulation with no oscillations. The dotted lines show the best fit for neutrino oscillation parameters describing this data. (Reprinted figure from [1] with permission from the APS).

$\Delta m^2 \approx 10^{-3}$–$10^{-4}$ $(\text{eV})^2$. Fits to the atmospheric (atm) data give the following parameters for two generations of flavor oscillations [2]:

$$|\Delta m^2_{\text{atm}}| \simeq 2.4 \times 10^{-3}\ \text{eV}^2 \quad \text{and} \quad \sin^2\theta_{\text{atm}} \simeq 0.5. \tag{6.14}$$

Although the first measurements of neutrino oscillations were obtained from atmospheric data, the parameters are within the range that can be tested with accelerator-based neutrino sources. The neutrino oscillations seen in atmospheric data were confirmed in muon disappearance measurements by the K2K experiment in Japan and the MINOS experiment, an accelerator-based experiment with neutrino beams produced from a proton beam hitting a fixed target at Fermilab in Chicago and directed to a detector in Soudan, Minnesota, 700 km away. Furthermore, not only are there accelerator-based measurements for muon diasspearance, there is now direct evidence for τ-lepton appearance, measured by the OPERA experiment in the CERN-Gran Sasso beam, as predicted by three-flavor neutrino oscillation parameters described below.

6.1.2 *Reactor Neutrino Experiments*

A nuclear reactor is an abundant source of antineutrinos. The number of fissions per second of ^{235}U in a commerical reactor is a few times 10^{19} with approximately two detectable antineutrinos produced per fission. The antineutrinos come from a cascade of β decays from neutron-rich fission products. Reactor antineutrinos, $\bar{\nu}_e$, typically have energies of a few MeV, well above the threshold to produce electrons in the final state, and are detected through the reaction $\bar{\nu}_e + p \to e^+ + n$. In the rapid oscillation scenario in equation (6.13)

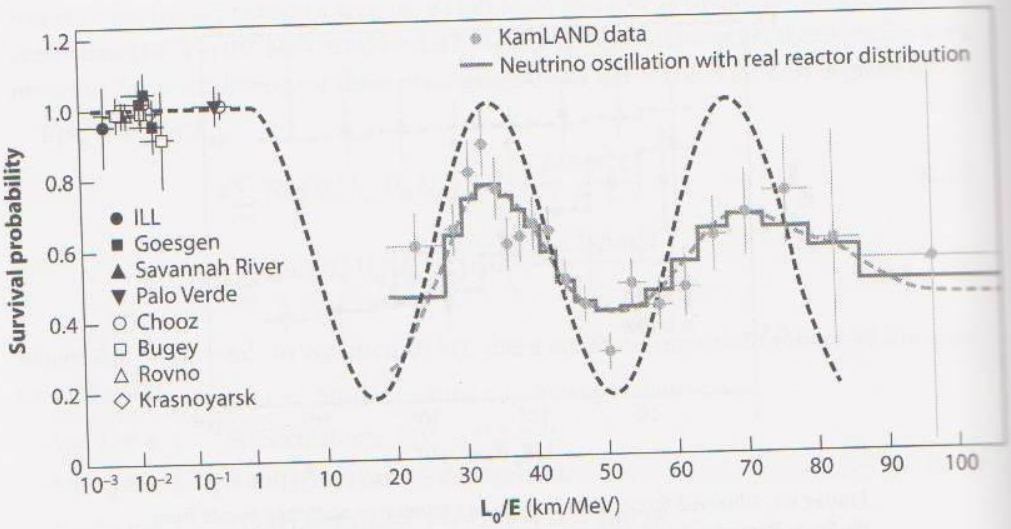

FIGURE 6.2. Survival probability of electron antineutrinos as a function of the effective L_0/E with an average reactor distance of $L_0 = 180$ km (Credit: KamLAND) [3]. The dotted line shows the best-fit oscillation parameters to the KamLAND data showing that the data are collected in a region of rapid oscillations. The solid line is a fit to the measured data including finite smearing effects from real reactor distributions.

for a fixed L, the expectation is to observe a drop in the rate of antineutrino interactions in the detector. The KamLAND long-baseline reactor experiment (average reactor distance is 180 km) measured an oscillation signature with a detected $\bar{\nu}_e$ rate which dips to ~60% of the predicted no oscillation rate, giving a best fit of

$$|\Delta m^2_{\text{reactor}}| \simeq 7.6 \times 10^{-5}\ \text{eV}^2 \quad \text{and} \quad \sin^2\theta_{\text{reactor}} \simeq 0.3 \tag{6.15}$$

when interpreted in terms of two-flavor neutrino oscillations [2]. The KamLAND data and data compiled for short-baseline reactor neutrino experiments are shown in figure 6.2 [3].

6.1.3 Solar Neutrino Data

In the case of the solar neutrinos, the effect of neutrinos propagating through the dense material of the sun has an important effect on the oscillation measurements. Electron neutrinos propagating through matter experience coherent forward scattering due to t-channel charged-current scattering. Matter effects were predicted by Mikheyev, Smirnov, and Wolfenstein (MSW) and are generally referred to as *MSW effects*. As a result of the interaction with atomic electrons, the electron neutrino flavor is constantly being regenerated by the weak interaction. As the weak interaction has a finite mass W propagator, the cross section for neutrino scattering grows with increasing neutrino energy for scattering momentum transfers small compared to M_W. Therefore, the matter effects increase with neutrino momentum. A relatively wide range of neutrino energies is emitted by the sun, as shown in figure 6.3 [4]. The various solar neutrino experiments have also had a range of sensitivies to these fluxes with the gallium experiments reaching the lowest thresholds

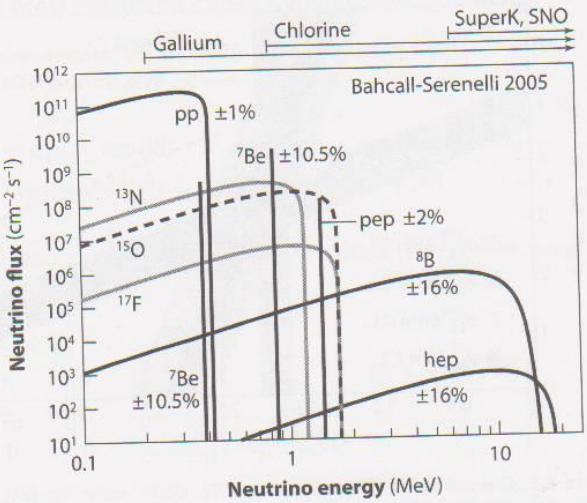

FIGURE 6.3. Solar neutrino energy spectrum predicted by the Standard Solar Model (2005). The uncertainties on the fluxes are quoted, and the detection thresholds for various solar neutrino experiments are shown at the top. (Reproduced by permission of the AAS) [4].

and the water Cherenkov experiments (SuperK) at the high end. The Sudbury Neutrino Observatory (SNO) developed a technique for flavor-independent detection of the neutrino flux from the sun where they measured the processes

$$\begin{aligned} \nu_e + d &\to p + p + e^- \quad (CC), \\ \nu_x + d &\to p + n + \nu_x \quad (NC), \\ \nu_x + e^- &\to \nu_x + e^- \quad (ES), \end{aligned} \tag{6.16}$$

and with this data accurately verified the total flux predictions with the Standard Solar Model in the neutrino energy region corresponding to the SuperK measurements, as shown in figure 6.4. The combination of SNO and SuperK data makes an astounding confirmation of the flux prediction and the vacuum oscillation parameter θ_{12} when corrected for matter (MSW) effects described below.

The effect on the propagation of neutrinos through matter is the addition of an effective index of refraction n given by

$$\begin{aligned} \exp(i(npz - Et)) &= \exp(i(pz - \sqrt{2}\,G_F N_e z - Et)) \\ &= \exp(iE(z - t))\exp\left(-i\left(\frac{m^2}{2p} + \sqrt{2}\,G_F N_e\right)z\right) \end{aligned} \tag{6.17}$$

for an electron neutrino propagating along the z-direction. If we define $m_0^2 = 2\sqrt{2}G_F N_e p$, then the effect on the mixing angle in matter θ'_{12} compared to the vacuum mixing angle θ_{12} is given by

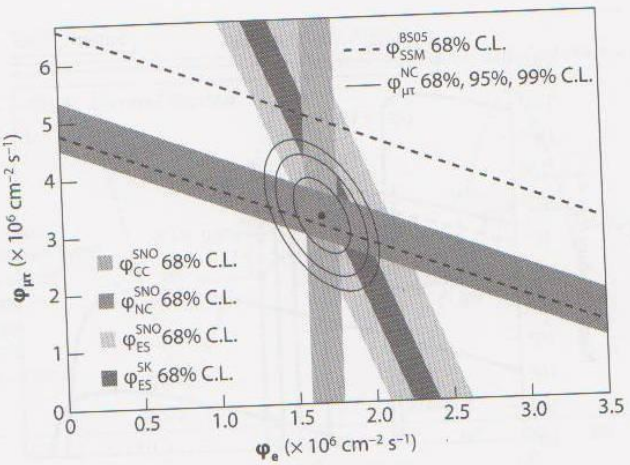

FIGURE 6.4. Comparison of charged-current (CC), elastic scattering (ES) and neutral-current (NC) neutrino fluxes measured by the SNO experiment and including Super-Kamiokande data (Credit: PDG) [2]. The neutral current is sensitive to all neutrino flavors and confirms the total predicted flux from the Standard Solar Model from figure 6.3.

$$\sin^2 2\theta'_{12} = \frac{\sin^2 2\theta_{12}}{\left[\left(\frac{m_0^2}{m_2^2 - m_1^2} - \cos 2\theta_{12}\right)^2 + \sin^2 2\theta_{12}\right]} \tag{6.18}$$

which for $m_0^2 \gg |m_2^2 - m_1^2|$, $\theta'_{12} \to 0$ and neutrinos fall into mass eigenstates while for $m_0^2 \ll |m_2^2 - m_1^2|$, $\theta'_{12} \to \theta_{12}$ and neutrinos undergo vacuum oscillations. Therefore, for the solar neutrino oscillation measurements, only the lowest energy electron neutrinos, those detected by ^{71}Ga experiments, are unaffected by matter effects for the bulk of the detected flux. The ^{71}Ga solar neutrino data give a value of θ_{12} in agreement with the reactor data. For ^{8}B neutrinos, the matter effects are large and the electron neutrinos will remain as an electron-neutrino weak eigenstate during regeneration and then adiabatically follow one of the mass eigenstates as the neutrinos propagate out of the sun and the density slowly decreases. The emerging neutrinos will remain in the mass eigenstate until they propagate to Earth and are detected. The ^{8}B neutrino measurements are, therefore, a static measurement of fixed neutrino mass eigenstates projected onto weak eigenstates. An important property of the denominator of equation (6.18) is the possibility to determine the sign of the squared mass difference $\Delta m_{21}^2 = m_2^2 - m_1^2$ for nonzero $\cos 2\theta_{12}$. For $\Delta m_{21}^2 > 0$ there is a cancellation in the denominator and, therefore, an enhancement in the matter oscillations relative to the vacuum $\sin^2 2\theta'_{12} > \sin^2 2\theta_{12}$. As both the gallium and reactor data set a baseline for the vacuum oscillation probability, the matter enhancement seen in the ^{8}B neutrinos fixes the sign of Δm_{21}^2 as positive where the lighter of the pair of mass states is more "electronlike" while the heavier is found to be a nearly equal admixture of all three neutrino flavors. Correcting for the solar MSW effect, the vacuum θ_{12} value agrees with the chlorine and Cherenkov detector solar neutrino data. The combined fit of solar and reactor data gives $\tan^2\theta_{12} = 0.47 \pm 0.05$ with $\Delta m_{21}^2 = +(7.6 \pm 0.2) \times 10^{-5}$ eV^2 [2].

6.1.4 Neutrino Mass Hierarchy, Flavor Content, and Potential for CP Violation

In a three-neutrino system, we write the general mixing matrix $U \equiv (U_L^{\nu})^{\dagger}$ as

$$U = \begin{pmatrix} c_{12}c_{13} & s_{12}c_{13} & s_{13}\exp(-i\delta) \\ -s_{12}c_{23} - c_{12}s_{23}s_{13}\exp(i\delta) & c_{12}c_{23} - s_{12}s_{23}s_{13}\exp(i\delta) & s_{23}c_{13} \\ s_{12}s_{23} - c_{12}c_{23}s_{13}\exp(i\delta) & -c_{12}c_{23} - s_{12}c_{23}s_{13}\exp(i\delta) & c_{23}c_{13} \end{pmatrix} \tag{6.19}$$

where $s_{ij} = \sin\theta_{ij}$ and $c_{ij} = \cos\theta_{ij}$ with $j > i$. The matrix (6.19) decomposes into the matrix product

$$\begin{aligned} U &= U_{12} \times U_{23} \times U_{13} \\ &= \begin{pmatrix} c_{12} & s_{12} & 0 \\ -s_{12} & c_{12} & 0 \\ 0 & 0 & 1 \end{pmatrix} \begin{pmatrix} 1 & 0 & 0 \\ 0 & c_{23} & s_{23} \\ 0 & -s_{23} & c_{23} \end{pmatrix} \begin{pmatrix} c_{13} & 0 & s_{13}\exp(-i\delta) \\ 0 & 1 & 0 \\ -s_{13}\exp(i\delta) & 0 & c_{13} \end{pmatrix} \end{aligned} \tag{6.20}$$

showing explicitly the individual two-flavor mixing matrices. In the limit where θ_{13} is small, the last mixing matrix is approximately the identity matrix $U_{13} \approx I_3$ and we recover the two-flavor reactor $U_{12} \approx U_{\text{reactor}}$ and atmospheric $U_{23} \approx U_{\text{atm}}$ mixing matrices. This approximation is verified below.

The small squared mass difference describing the reactor oscillation data and the factor of 30 larger squared mass difference found in atmospheric oscillation data imply that Nature has chosen a set of mass splittings such that $|\Delta m^2_{13}| \simeq |\Delta m^2_{23}| \gg |\Delta m^2_{12}|$. Two possible neutrino mass hierarchy scenarios based on these parameters are shown in figure 6.5, labeled arbitrarily as the normal and inverted hierarchies. In this situation, the oscillation formula (6.9) simplifies, for $\alpha \neq \beta$, to

$$P(\nu_\alpha \to \nu_\beta) = 4\left|U^*_{\alpha 3}\, U_{\beta 3}\right|^2 \sin^2\left(\frac{\Delta m^2_{23} t}{4p}\right) \tag{6.21}$$

using the unitarity of the three-generation U matrix and assuming that $\Delta m^2_{12} t/p$ is small compared to unity. This results in the following expected oscillation probabilities:

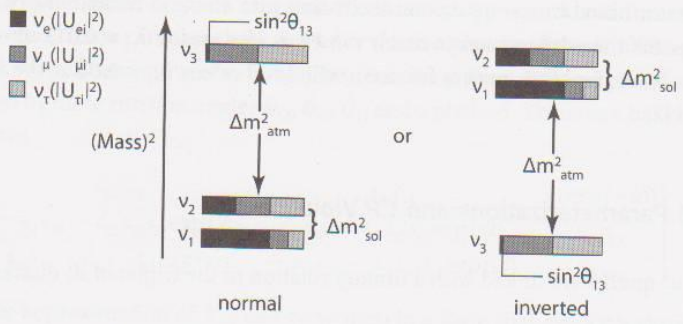

FIGURE 6.5. Two possible neutrino mass hierarchy scenarios, arbitrarily labeled as the *normal* and *inverted hierarchies* (Credit: B. Kayser).

$$P(\nu_e \to \nu_\mu) = \sin^2\theta_{23}\sin^2 2\theta_{13}\sin^2\left(\frac{\Delta m^2_{23}t}{4p}\right),$$
$$P(\nu_e \to \nu_\tau) = \cos^2\theta_{23}\sin^2 2\theta_{13}\sin^2\left(\frac{\Delta m^2_{23}t}{4p}\right), \tag{6.22}$$
$$P(\nu_\mu \to \nu_\tau) = \cos^2\theta_{13}\sin^2 2\theta_{23}\sin^2\left(\frac{\Delta m^2_{23}t}{4p}\right).$$

However, the observed nonoscillation of the atmospheric electron neutrinos indicates that the $P(\nu_e \to \nu_\mu)$ and $P(\nu_e \to \nu_\tau)$ transition probabilities are suppressed. The atmospheric data indicate from muon neutrino disappearance measurements that [2]

$$|\Delta m^2_{23}| \simeq 2.4 \times 10^{-3}\ \text{eV}^2,\ \cos^2\theta_{13}\sin^2 2\theta_{23} \simeq 1. \tag{6.23}$$

The combination of this data points to a small value of θ_{13} giving a $\sin^2 2\theta_{13}$ suppression of $P(\nu_e \to \nu_\mu)$ and $P(\nu_e \to \nu_\tau)$ while $\theta_{23} \simeq 45°$. For θ_{13} small, $\theta_{13} < 10°$, the U matrix can be simplified to

$$U = \begin{pmatrix} c_{12} & s_{12} & \theta_{13}\exp(-i\delta) \\ -s_{12}c_{23} & c_{12}c_{23} & s_{23} \\ s_{12}s_{23} & -c_{12}c_{23} & c_{23} \end{pmatrix}. \tag{6.24}$$

Figure 6.5 shows the flavor composition based on U of the three neutrino mass eigenstates, indicating that each mass eigenstate behaves differently with respect to lepton flavor conservation with one "electronlike," one μ-τ biflavor, and one all-flavor mixture. As shown in the figure, the electronlike neutrino is known to be lighter than the all-flavor neutrino mass eigenstate due to the enhancement in the mixing probability from the MSW effect observed in the solar neutrino data.

To measure CP violation in the neutrino sector, as evidenced by the possible nonzero complex phase δ in equation (6.24), requires a measurement to determine that θ_{13} is nonzero, as this is the linear coefficient to the leading CP-violating term. Future experiments, such as Daya Bay, with more precise reactor neutrino data on $\bar{\nu}_e$ disappearance provide a promising avenue to place further constraints on or measure θ_{13}. Similarly, electron neutrino appearance experiments, such as NOνA and T2K, aim to detect accelerator-based muon neutrinos oscillating into electron neutrinos. The expected sensitivities for these experiments reach values as low as $\sin^2\theta_{13} = 0.01$, where current constraints from the MNS matrix fits are at the level of $\sin^2\theta_{13} < 0.04$ at the 90% confidence level [2].

6.2 CKM Parameterizations and *CP* Violation

The three u^i_L quarks are linked with a unitary rotation of the triplet of d^i_L quarks

$$V_{UD} = U^u_L (U^d_L)^\dagger. \tag{6.25}$$

The matrix V_{UD} is known as the *Cabibbo-Kobayashi-Maskawa* (CKM) mixing matrix. The values of the matrix indicate how much of the charged-current coupling is shared between the three generations of up-type and down-type quarks, where

$$j^{\mu}_{CC} = \frac{1}{\sqrt{2}} \bar{\Psi}^{U}_{L} \gamma^{\mu} V_{UD} \Psi^{D}_{L} + \frac{1}{\sqrt{2}} \bar{\Psi}^{D}_{L} \gamma^{\mu} V^{*}_{UD} \Psi^{U}_{L} \tag{6.26}$$

with

$$V_{UD} = \begin{pmatrix} V_{ud} & V_{us} & V_{ub} \\ V_{cd} & V_{cs} & V_{cb} \\ V_{td} & V_{ts} & V_{tb} \end{pmatrix}. \tag{6.27}$$

If we consider for the moment only two mass generations, then the general unitary matrix has four parameters and can generally be written in the form

$$V^{(2)}_{UD} = \begin{pmatrix} \exp(i\phi_1)\cos\theta & \exp(i(\phi_1 + \phi_2))\sin\theta \\ -\exp(i\phi_3)\sin\theta & \exp(i(\phi_2 + \phi_3))\cos\theta \end{pmatrix}. \tag{6.28}$$

We can rewrite the 2×2 matrix as

$$\begin{pmatrix} \exp(i\phi_1) & 0 \\ 0 & \exp(i\phi_3) \end{pmatrix} \begin{pmatrix} \cos\theta & \sin\theta \\ -\sin\theta & \cos\theta \end{pmatrix} \begin{pmatrix} 1 & 0 \\ 0 & \exp(i\phi_2) \end{pmatrix}. \tag{6.29}$$

Notice that the matrices involving ϕ_1, ϕ_2, and ϕ_3 are diagonal. These phases simply multiply the individual quark wave functions and by redefinition of the wave functions can be absorbed without changing any physical quantity. The rotation angle θ, however, cannot be removed by redefinition of the quark phases and is the one physical parameter of the two-generation CKM matrix. This angle is denoted θ_C, the Cabibbo angle. The numerical values of the $V^{(2)}_{UD}$ elements are [2]

$$\sin\theta_C = 0.225 \pm 0.001, \quad \text{implying that} \quad \cos\theta_C = 0.975. \tag{6.30}$$

Thus, weak decay rates involving a $u \leftrightarrow s$ quark transition are suppressed by a factor $\sin^2\theta_C = 0.05$, or 5%. The Cabibbo-angle two-generation description is a good estimate (better than 1%) for light-quark transitions.

For three generations of quark families, the three up-type-quark and three down-type-quark wave functions can absorb $2 \cdot 3 - 1 = 5$ relative phases of the 3^2 CKM parameters with quark wave function redefinitions. The remaining four physical parameters can be represented by three rotation angles θ_{12}, θ_{13}, θ_{23} and a phase δ. These can be written in the general form

$$V_{UD} = \begin{pmatrix} c_{12}c_{13} & s_{12}c_{13} & s_{13}\exp(-i\delta) \\ -s_{12}c_{23} - c_{12}s_{23}s_{13}\exp(i\delta) & c_{12}c_{23} - s_{12}s_{23}s_{13}\exp(i\delta) & s_{23}c_{13} \\ s_{12}s_{23} - c_{12}c_{23}s_{13}\exp(i\delta) & -c_{12}c_{23} - s_{12}c_{23}s_{13}\exp(i\delta) & c_{23}c_{13} \end{pmatrix}. \tag{6.31}$$

An accurate approximation of V_{UD} can be written in a form that explicitly shows the suppression of the off-diagonal elements progressively with each mass generation, as we

know must occur based on the accuracy of the Cabibbo angle description for the light-quark flavors. This is achieved by defining

$$\begin{aligned} s_{12} &= \sin\theta_C = \lambda,\ s_{23} = A\lambda^2 \ll s_{12}, \\ s_{13}\exp(-i\delta) &= A\lambda^3(\rho - i\eta) \ll s_{23} \text{ in magnitude}, \\ V_{UD} &= \begin{pmatrix} 1-\lambda^2/2 & \lambda & A\lambda^3(\rho - i\eta) \\ -\lambda & 1-\lambda^2/2 & A\lambda^2 \\ A\lambda^3(1-\rho-i\eta) & -A\lambda^2 & 1 \end{pmatrix}. \end{aligned} \tag{6.32}$$

Equation (6.32) is known as the *Wolfenstein parameterization* of the CMS matrix. The terms in the matrix are measured in various weak decay processes. The term $V_{cb} = A\lambda^2$ is measured in $B^{\pm}$ meson decay with a $b \to c$ transition. This gives a value of $|V_{cb}| = 0.0415 \pm 0.001$, which for $\lambda = 0.225 \pm 0.001$ gives $A = 0.81 \pm 0.02$ [2]. The measurement of V_{ub} is determined from the $3^{rd} \to 1^{st}$ generation $b \to u$ transition, neutral B meson mixing, and CP-violating asymmetries and provides a measurement of ρ and η [2]:

$$\rho = 0.14 \pm 0.03 \quad \text{and} \quad \eta = 0.35 \pm 0.02. \tag{6.33}$$

The values of λ, A, ρ, and η are constrained by several measurements. A compact representation for testing the self-consistency of the CKM matrix element measurements is in the form of the unitarity triangle. There are, in fact, six possible unitarity triangles corresponding to the off-diagonal zeros of the unitarity condition $V_{UD}V_{UD}^{\dagger} = 1$, namely,

$$\sum_i V_{ij}V_{ik}^* = 0 \quad \text{for nonidentical columns } (j \neq k), \tag{6.34}$$

and

$$\sum_i V_{ji}V_{ki}^* = 0 \quad \text{for nonidentical rows } (j \neq k), \tag{6.35}$$

where the V_{ij} are the elements of the CKM matrix. A particularly symmetric configuration of legs in the triangle comes from choosing the product terms $V_{ij}V_{ik}^*$ to be of the same order in powers of λ. There are two triangles with all legs with a length of order λ^3 and these are given by

$$\begin{aligned} V_{ud}V_{ub}^* + V_{cd}V_{cb}^* + V_{td}V_{tb}^* &= 0, \\ V_{ud}V_{td}^* + V_{us}V_{ts}^* + V_{ub}V_{tb}^* &= 0. \end{aligned} \tag{6.36}$$

In the study of B-meson decays, the V_{cb} term is particularly important and, therefore, the first of these triangles is commonly known as the *unitarity triangle*. The legs of the unitarity triangle can be normalized by the middle term (V_{cb} containing) of equation (6.36) to give an apex at $(\rho, i\eta)$, as shown in figure 6.6.

The connection between the η parameter and CP violation can be seen by comparing terms in the electroweak Lagrangian under discrete transformations. We can, therefore, examine the terms generated by equation (6.26) in weak charged-current processes. The term $\bar{\Psi}_L^U \gamma^\mu V_{UD} \Psi_L^D W_\mu^+$ are interactions with a V_{UD} coefficient describing a d-quark emitting or absorbing a W boson and rotating into a u-quark, an anti-u-quark emitting or

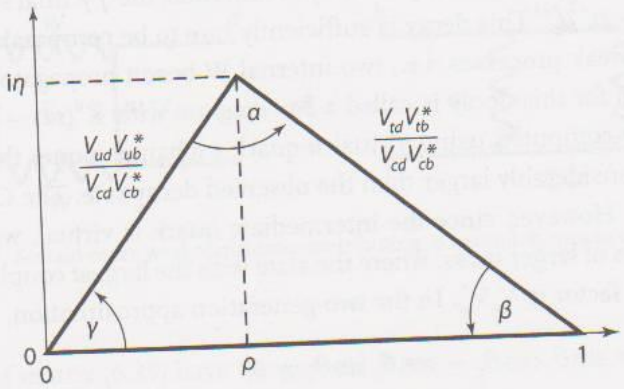

FIGURE 6.6. The unitarity triangle.

absorbing a W boson and rotating into an anti-d-quark, a d-quark annihilating with an anti-u-quark and the pair production of a u-quark and an anti-d-quark. All of these interactions involve elements of V_{UD} (not V_{UD}^*). The corresponding Hermitian conjugate terms (taking up-type quarks to down-type quarks) involve elements of V_{UD}^*. Returning to the properties of the weak charged-current interaction under discrete symmetry operations, the operation of C takes the particle $SU(2)_{\text{flavor}}$ doublet to the antiparticle doublet and maps $u_L \to -\bar{d}_R$ and $d_L \to \bar{u}_R$, i.e., the $SU(2)_{\text{flavor}}$ doublet transforms as

$$\begin{pmatrix} u \\ d \end{pmatrix} \xrightarrow{C} \begin{pmatrix} -\bar{d} \\ \bar{u} \end{pmatrix}, \tag{6.37}$$

but in weak isospin the left-handed chirality u_L quarks are part of $SU(2)_L$ doublets while the right-handed chirality $\bar{d}_R$ quarks are singlets. Therefore, the separate operations of C or P change the chiral gauge charges and generate terms that do not exist in the $SU(2)_L \times U(1)_Y$-invariant electroweak Lagrangian. Applying the combined operation of CP to the term $\bar{\Psi}_L^U \gamma^\mu V_{UD} \Psi_L^D$ yields the CP-transformed processes with V_{UD} coefficients. However, the Hermitian conjugate processes in the Lagrangian have V_{UD}^* coefficients. Therefore, if V_{UD} contains imaginary terms, i.e., $V_{UD} \neq V_{UD}^*$, then CP symmetry is violated in the $SU(2)_L \times U(1)_Y$ interaction with corresponding violations in time-reversed processes.

6.3 Box Diagrams and the GIM Mechanism

The off-diagonal elements of the CKM matrix correspond to rare transitions. The study of rare decays is, therefore, one means of evaluating the couplings to heavy mass states. This effect was used by Glashow, Iliopoulos, and Maiani (GIM) to predict the mass of the charm quark before its discovery. This analysis was first applied to the decay branching fraction of $K_L^0 \to \mu^+\mu^-$, which was measured to be 7.3×10^{-9}. The K_L^0 is nearly CP odd and, therefore, can mix with the light pseudoscalars π^0, η and η' through diagrams with one internal W boson propagator. As with the light $J^P = 0^-$ states, the K_L^0 has a small nonzero

decay rate to $\gamma\gamma$. In order for the K_L^0 to decay to dimuons, the $\gamma\gamma$ final state must rescatter to give $K_L^0 \to 2\gamma \to \mu^+\mu^-$. This decay is sufficiently rare to be comparable to second-order charged-current weak processes, i.e., two internal W boson propagators. The second-order weak diagram for this decay is called a *box diagram* with $\bar{K}^0(s\bar{d}) \to W^{+*}W^{-*} \to \mu^+\mu^-$. If the diagram is computed using virtual u-quark exchange alone, then the amplitude for the decay is considerably larger than the observed decay rate. The CKM factor for the u-quark is $V_{us}V_{ud}^*$. However, since the intermediate quark is virtual, we need to include intermediate states of larger mass, where the state with the largest coupling is the c-quark. The c-quark CKM factor is $V_{cs}V_{cd}^*$. In the two-generation approximation,

$$V_{us}V_{ud}^* + V_{cs}V_{cd}^* = \sin\theta_C\cos\theta_C - \cos\theta_C\sin\theta_C = 0, \tag{6.38}$$

by unitarity of the matrix. Thus, the amplitude from the box diagram is suppressed due to a cancellation between u and c quarks. This is known as the *GIM mechanism*. The t-quark CKM factors are very small and do not contribute significantly to the amplitude. However, for box diagrams involving initial b-quarks instead of s-quarks, the CKM factors are much larger for the virtual t-quark contribution. As a result, virtual t-quarks typically provide the dominant amplitude, compared to u and c exchange, for box diagrams in the B-meson system.

6.4 Neutral Meson Oscillations and *CP* Violation

The mixing of particle and antiparticle neutral meson states comes from second-order weak transitions that connect the two states through common virtual or real intermediate states, as shown in figure 6.7. The virtual states contribute to the mass of the mesons while the real states contribute to the partial width according to the complex mass matrix

$$i\frac{\partial}{\partial t}\begin{pmatrix} B^0 \\ \bar{B}^0 \end{pmatrix} = \left(M - \frac{i}{2}\Gamma\right)\begin{pmatrix} B^0 \\ \bar{B}^0 \end{pmatrix} = \begin{pmatrix} m - \frac{i}{2}\Gamma & \Delta m_{12} - \frac{i}{2}\Gamma_{12} \\ \Delta m_{12}^* - \frac{i}{2}\Gamma_{12}^* & m - \frac{i}{2}\Gamma \end{pmatrix}\begin{pmatrix} B^0 \\ \bar{B}^0 \end{pmatrix}. \tag{6.39}$$

The diagonal terms describe the decay of the neutral B mesons with m being the mass of the flavor eigenstates B^0 and $\bar{B}^0$ and Γ their common decay width before the weak interaction is turned on. The second-order weak interaction introduces off-diagonal terms in the complex mass matrix (6.39) and is responsible for B^0–$\bar{B}^0$ transitions. Thus, the weak interaction results in a new set of mass eigenstates and total widths, changing m and Γ for the physical states. The heavy (H) and light (L) states have mass and width splittings given by

$$\begin{aligned} \Delta m \equiv M_H - M_L &= 2\mathcal{R}e\sqrt{\left(\Delta m_{12} - \frac{i}{2}\Gamma_{12}\right)\left(\Delta m_{12}^* - \frac{i}{2}\Gamma_{12}^*\right)}, \\ \frac{\Delta\Gamma}{2} \equiv \frac{\Gamma_H}{2} - \frac{\Gamma_L}{2} &= -2\mathcal{I}m\sqrt{\left(\Delta m_{12} - \frac{i}{2}\Gamma_{12}\right)\left(\Delta m_{12}^* - \frac{i}{2}\Gamma_{12}^*\right)}. \end{aligned} \tag{6.40}$$

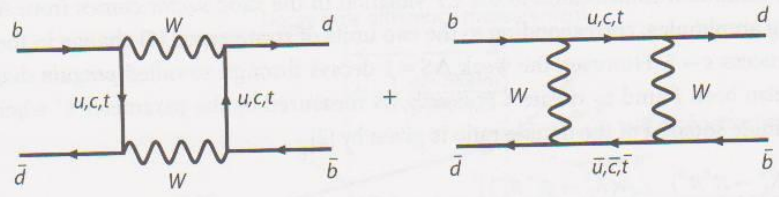

FIGURE 6.7. Second-order weak transitions contributing to neutral B_d-meson oscillations.

The eigenstates of matrix (6.39) have the general form

$$|P_L\rangle = p|P^0\rangle + q|\bar{P}^0\rangle, \qquad |P_H\rangle = p|P^0\rangle - q|\bar{P}^0\rangle \tag{6.41}$$

where p and q are complex constants that satisfy $|p|^2 + |q|^2 = 1$. The ratio of q/p is found by diagonalizing (6.39) and is given by

$$\frac{q}{p} = \sqrt{\frac{\Delta m_{12}^* - i\Gamma_{12}^*/2}{\Delta m_{12} - i\Gamma_{12}/2}}. \tag{6.42}$$

The operation of CP gives

$$CP|P^0\rangle \to \eta_{CP}|\bar{P}^0\rangle \tag{6.43}$$

where we can choose $\eta_{CP} = -1$. In the absence of CP violation, CP eigenstates are formed and the coefficients are equal and given by

$$p = q = \frac{1}{\sqrt{2}}, \tag{6.44}$$

corresponding to

$$|P^0_{CP=\pm 1}\rangle = \frac{1}{\sqrt{2}}\left(|P^0\rangle \mp |\bar{P}^0\rangle\right). \tag{6.45}$$

The physical states in the presence of the weak interaction are, therefore, an admixture of particle and antiparticle neutral meson flavor eigenstates. A similar mass matrix occurs in the K^0–$\bar{K}^0$ system where the short-lived (S) state decays primarily to the CP-even 2π final state and the long-lived state (L) decays to the CP-odd 3π final state. The lifetime difference in the physical kaon states is mainly due to the size of the phase space for CP-conserving $n\pi$ decays, namely, $K_S^0 \to 2\pi$ and $K_L^0 \to 3\pi$. The first evidence for CP violation was observed in 1964 by Fitch, Cronin, et al. in the decay $K_L^0 \to \pi^+\pi^-$ far downstream the beam line from the region of $K_S^0 \to \pi^+\pi^-$ decays. The magnitude of the ratio of the amplitudes for K_L^0 and K_S^0 decay to $\pi^+\pi^-$ is approximately given by [1]

$$|\epsilon_K| = \left|\frac{p-q}{p+q}\right| \approx \left|\frac{A(K_L^0 \to \pi^+\pi^-)}{A(K_S^0 \to \pi^+\pi^-)}\right| = (2.28 \pm 0.011) \times 10^{-3}. \tag{6.46}$$

The dominant contribution to the *CP* violation in the kaon sector comes from $\Delta S = 2$ mixing amplitudes, corresponding to the two units of strangeness (S) change in the mixing process $s \to \bar{s}$. However, the weak $\Delta S = 1$ decays through so-called *penguin diagrams* have also been found to violate *CP directly*, as measured by the parameter ϵ' where the magnitude squared of the double ratio is given by [2]

$$\left|\frac{A(K_L^0 \to \pi^0\pi^0)}{A(K_S^0 \to \pi^0\pi^0)} \Big/ \frac{A(K_L^0 \to \pi^+\pi^-)}{A(K_S^0 \to \pi^+\pi^-)}\right|^2 \approx 1 - 6\epsilon'/\epsilon \tag{6.47}$$

with

$$\epsilon'/\epsilon = (1.65 \pm 0.26) \times 10^{-3}. \tag{6.48}$$

In the neutral B-meson systems, there are many possibilities for the observation of *CP* violation. Direct *CP* violation, for example, is observed in the decay rate asymmetry of $B_d^0 \to K^+\pi^-$ as compared to $\bar{B}_d^0 \to K^-\pi^+$ at the level of 10%, almost two orders of magnitude larger than in the $\pi\pi$ decays of kaons. However, the branching fraction of the B_d^0 meson to $K^+\pi^-$ is approximately 2×10^{-5} and therefore the production of 10^8 or more neutral B mesons is needed to study this decay mode. Proton-proton and proton-antiproton colliders are copious sources of B mesons, inclusively produced in hadronic interactions. Hadron colliders are described in more detail in chapter 8. Another source of B mesons is from the correlated B–$\bar{B}$ decays of the $\Upsilon(4S)$ and $\Upsilon(5S)$ resonances, where the time evolution of the correlated pair introduces additional methods to measure the CKM parameters. In particular, B-meson pairs from $\Upsilon(4S)$ decay have been studied extensively at two asymmetric e^+e^- collider experiments, the BaBar experiment at PEP-II and the Belle experiment at KEKB.

A neutral B-meson oscillation experiment begins by creating a correlated pair of B^0–$\bar{B}^0$ mesons from the decay of an upsilon resonance, $\Upsilon(4S) \to B^0\bar{B}^0$. In an asymmetric e^+e^- collider, the electron and positron beam energies are unequal and, therefore, the Υ resonance is boosted in the lab frame. This boost allows the experiment to measure the time difference between the decaying B mesons, as shown in figure 6.8. The first meson to decay is "flavor" tagged according to its decay products. At this reference time, the second B meson is known to be in either a pure B^0 or $\bar{B}^0$ state. The difference in decay length along the beam direction is then translated into a proper time difference in the rest frame of the second B meson. Thus, the time evolution of the probability to find the second meson in the same state or the opposite state is given by (with $|q/p| = 1$)

$$|f_\pm(t)|^2 = \frac{1}{2}\exp(-\Gamma t)\left(\cosh\left(\frac{\Delta\Gamma}{2}t\right) \pm \cos(\Delta m t)\right) \tag{6.49}$$

where the plus sign indicates the same state and the minus sign the opposite state, according to

$$\begin{aligned} |B^0(t)\rangle &= f_+(t)|B^0\rangle + f_-(t)\frac{q}{p}|\bar{B}^0\rangle, \\ |\bar{B}^0(t)\rangle &= f_+(t)|\bar{B}^0\rangle + f_-(t)\frac{p}{q}|B^0\rangle. \end{aligned} \tag{6.50}$$

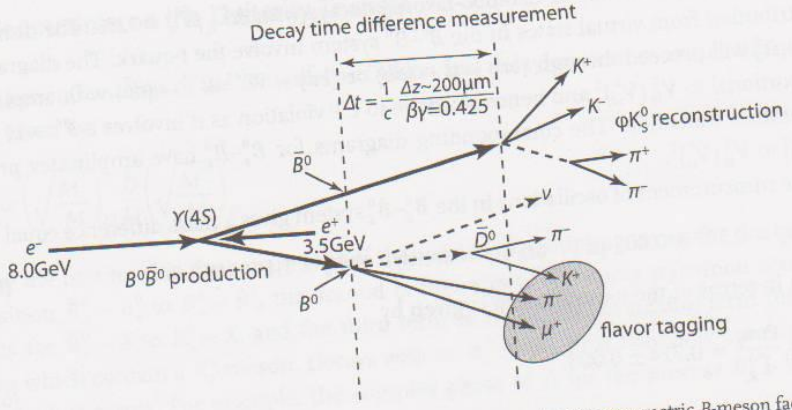

FIGURE 6.8. Neutral B-meson oscillation and decay measurements at an asymmetric B-meson factory (Credit: BABAR).

Equation (6.50) shows the explicit dependence of the mass difference Δm and the decay width difference $\Delta\Gamma$ of the heavy and light states.

If CP is conserved, then $\Delta m_{12} = \Delta m^*_{12}$ and $\Gamma_{12} = \Gamma^*_{12}$ and therefore $q/p = 1$. Deviations of q/p from unity indicate CP violation. If the magnitudes of $|q|$ and $|p|$ differ, then this is called *direct CP violation* and can be determined from the ratio of the decay amplitudes as in the ϵ'/ϵ measurement in the kaon system (6.47). It is more common to detect a phase difference between q and p and in order to be sensitive to a phase, two interfering amplitudes must be present. The most common technique is to use the interference of direct decay with oscillation plus decay for common decay modes, as sketched in figure 6.9. This method of measuring CP violation is called *indirect CP-violation*.

Unlike the K^0–$\bar{K}^0$ system, the B^0_d and $\bar{B}^0_d$ decays share few real transitions (decay modes). Common decay modes are Cabibbo suppressed, such as $b \to c(\bar{c}d)$ where the (W^-) decay is Cabibbo suppressed and similarly for $\bar{b} \to \bar{c}(c\bar{d})$. This implies that $\Delta\Gamma_{B_s} \ll \bar{\Gamma}_{B_s}$ where $\bar{\Gamma}_{B_s}$ is the average of the heavy and light B_d meson widths. There is a larger effect on the width

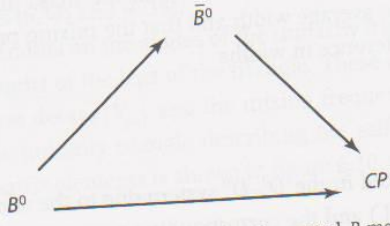

FIGURE 6.9. The direct decay amplitude of a neutral B meson to a CP eigenstate will interfere with a neutral meson that first oscillates to a $\bar{B}$ meson and then subsequently decays to the same final state.

in the B_s^0–$\bar{B}_s^0$ system due to Cabibbo-favored decays with $\Delta\Gamma_{B_s}/\bar{\Gamma}_{B_s} \approx 12\%$. The dominant contribution from virtual states in the B^0–$\bar{B}^0$ system involve the t-quark. The diagram for $\bar{B}_d^0 \to B_d^0$ will proceed through $(b\bar{d}) \to t\bar{t} \to (d\bar{b})$ or $(b\bar{d}) \to W^{+*}W^{-*} \to (d\bar{b})$ with amplitudes proportional to $V_{tb}^2(V_{td}^*)^2$ and hence sensitive to CP violation as it involves a $3^{rd} \to 1^{st}$ mass generation transition. The corresponding diagrams for B_s^0–$\bar{B}_s^0$ have amplitudes proportional to $V_{tb}^2(V_{ts}^*)^2$.

The measurement of oscillations in the B_d^0–$\bar{B}_d^0$ system gives a mass difference equal to [2]

$$\Delta m_d = 0.507 \pm 0.005 \text{ ps}^{-1} \quad \text{or, equivalently,} \quad \Delta m_d^2 \approx 1.1 \times 10^{-7} \text{ eV}^2, \tag{6.51}$$

which in terms of the natural width is given by

$$x_d = \frac{\Delta m_d}{\bar{\Gamma}_{B_d}} = 0.774 \pm 0.008. \tag{6.52}$$

The CDF and DØ experiments observed B_s^0–$\bar{B}_s^0$ mixing and due to the rapid oscillations of the states, the mass difference is given by [2]

$$\Delta m_s = 17.8 \pm 0.1 \text{ ps}^{-1} \quad \text{or, equivalently,} \quad \Delta m_s^2 \approx 1.4 \times 10^{-4} \text{ eV}^2, \tag{6.53}$$

also written as

$$x_s = \frac{\Delta m_s}{\bar{\Gamma}_{B_s}} = 26.2 \pm 0.5. \tag{6.54}$$

The value of x_s is predicted to be

$$\frac{|V_{ts}|^2}{|V_{td}|^2} = f_{SU(3)}^{-1} \frac{\Delta m_s}{\Delta m_d} \approx 25 \tag{6.55}$$

using an $SU(3)_{\text{flavor}}$ violation factor $f_{SU(3)} \approx 1.4$ that affects the comparison of the mixing parameters of the B_s and B_d states. The value of x_s is in agreement with a self-consistent CKM matrix description of quark mixing.

Oscillations have been observed in the neutral charm mesons D^0–$\bar{D}^0$ at the B-factories. The large rate of $D^{*\pm}$ production from B-hadron decay is used to tag the flavor $(D^0/\bar{D}^0)$ of the neutral D meson through the slow pion decay $D^{*\pm} \to \pi^{\pm} D^0$. The shape of the time-dependent distribution of the doubly Cabbibo–suppressed (DCS) decay $D^0 \to K^+\pi^-$ is analyzed for interference contributions from D^0–$\bar{D}^0$ mixing followed by the Cabbibo-favored (CF) decay $\bar{D}^0 \to K^+\pi^-$. The first indications are that the mass difference between the states is less than ~1% of the average width and that the mixing probability has a larger contribution from for the difference in widths

$$y = \frac{\Delta\Gamma}{2\Gamma} \approx 1\%. \tag{6.56}$$

Oscillations are less pronounced in the D^0–$\bar{D}^0$ system due to the short lifetime of the favored weak decay (increasing Γ) and the corresponding suppresion from CKM elements in the second-order weak transition (decreasing Δm).

6.5 Constraints on the Unitarity Triangle

In the general analysis of the B-meson oscillation and decay, one can construct the quantity Λ given by

$$\Lambda = \left(\sqrt{\frac{M^*}{M}}\right)_{B_x^0} \frac{\bar{D}}{D} \left(\sqrt{\frac{M^*}{M}}\right)_{K^0} \tag{6.57}$$

where the first term is the square root of the ratio of the coupling terms for the mixing transition $\bar{B}_x^0 \to B_x^0$ to $B_x^0 \to \bar{B}_x^0$, the second is the ratio of the decay transition coupling terms for $\bar{B}_x^0 \to X$ to $B_x^0 \to X$, and the third term is an additional mixing term for final states which contain a K_s^0 meson. Decays with no K_s^0 in the final state only have the first two product terms. For example, the complex phase of Λ for the process $B_d^0 \to \Psi K_s^0$ is given by

$$\begin{aligned} \Lambda(B_d^0 \to \Psi K_s^0) &= \left(\frac{V_{td}^* V_{tb}}{V_{td} V_{tb}^*}\right)\left(\frac{V_{cs}^* V_{cb}}{V_{cs} V_{cb}^*}\right)\left(\frac{V_{cd}^* V_{cs}}{V_{cd} V_{cs}^*}\right) \\ &= \exp\left(i2\tan^{-1}\left(\frac{\eta}{1-\rho}\right)\right) = \exp(i2\beta). \end{aligned} \tag{6.58}$$

For the process $B_d^0 \to \pi^+\pi^-$, the phase of Λ is given by

$$\begin{aligned} \Lambda(B_d^0 \to \pi^+\pi^-) &= \left(\frac{V_{td}^* V_{tb}}{V_{td} V_{tb}^*}\right)\left(\frac{V_{ud}^* V_{ub}}{V_{ud} V_{ub}^*}\right) \\ &= \exp\left(i2\tan^{-1}\left(\frac{\eta}{1-\rho}\right) - 2\tan^{-1}\left(\frac{\eta}{\rho}\right)\right) \\ &= \exp(i2(\beta-\gamma)) = \exp(i2(\alpha-\pi)) = \exp(-i2\alpha). \end{aligned} \tag{6.59}$$

The measurement of the third angle, γ, is most directly determined from B_s^0–$\bar{B}_s^0$ mixing and decay. The angles α, β, and γ are the internal angles of the unitarity triangle, as shown in figure 6.6. A nonzero area of the unitarity triangle indicates the presence of CP violation, i.e., the triangle collapses when the complex phase $\eta = 0$. In fact, the area of the unitarity triangle, denoted J, is approximately 25 standard deviations from zero and is invariant under the choice of triangle from the six possible unitarity conditions of the CKM matrix from equations (6.34) and (6.35).

In addition to constraints on the angles of the unitarity triangle, a number of measurements restrict the lengths of the legs of the triangle. These are ϵ_K from the kaon system, the $3^{rd} \to 1^{st}$ generation decays $|V_{ub}|$, and the mixing frequencies of the $B_x^0 - \bar{B}_x^0$ systems. The current fit to the unitarity triangle describing the self-consistency of the measurements of the CKM matrix elements is shown in figure 6.10, where relative to figure 6.6 we define

$$\bar{\rho} = \rho(1 - \lambda^2/2), \quad \bar{\eta} = \eta(1 - \lambda^2/2). \tag{6.60}$$

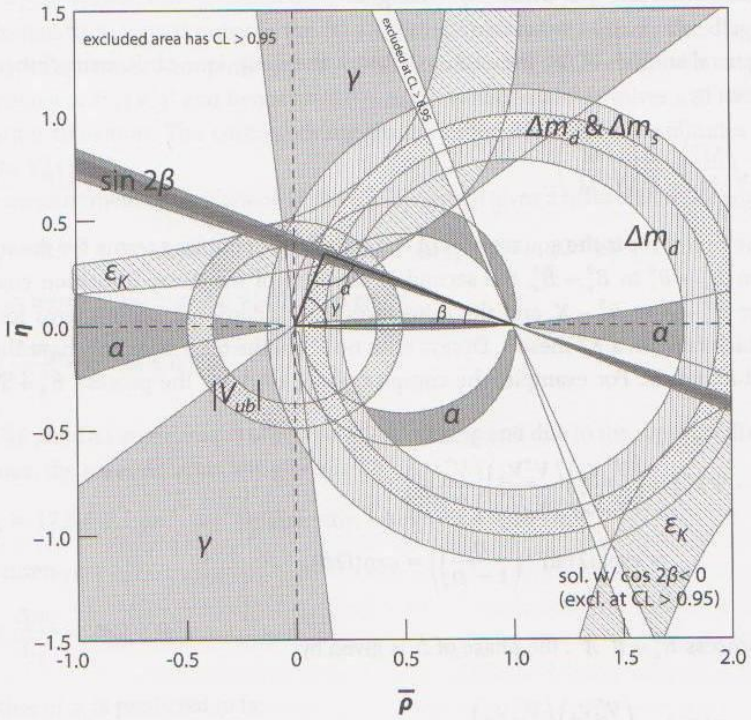

FIGURE 6.10. Fit to the unitarity triangle in the $(\bar{\eta}, \bar{\rho})$-plane indicating measurement constraints from α, $\sin 2\beta$, γ, ϵ_K, $|V_{ub}|$, Δm_d and Δm_s (Credit: CKMfitter) [5].

6.6 Exercises

1. **SuperK.** The SuperKamiokande experiment sees evidence for flavor oscillations in neutrinos produced in the atmosphere by cosmic rays. One interpretation is that the deficit in observed muon neutrinos is the result of $\nu_\mu \to \nu_\tau$ mixing. Using a two-generation mixing model, the $\nu_\mu \to \nu_\tau$ mixing probability is given by

$$P(\nu_\mu \to \nu_\tau) = \sin^2(2\theta)\sin^2\left(\frac{\Delta m^2 L}{4E}\right)$$

where θ is the mixing angle between flavor and mass eigenstates, Δm^2 is the difference between the masses squared of the mass eigenstates, E is the neutrino energy, and L is the distance from the source, in units where $\hbar = c = 1$. The term $\sin^2(2\theta)$ is referred to as the amplitude of the oscillations. SuperK's results, interpreted in this model, give $\Delta m^2 \approx 2.4 \times 10^{-3}$ eV^2, $\sin^2(2\theta) \approx 1$.

However, there are three known generations of neutrinos. Thus, in general, mixing will be governed by a 3×3 mixing matrix

$$U = \begin{pmatrix} U_{e1} & U_{e2} & U_{e3} \\ U_{\mu 1} & U_{\mu 2} & U_{\mu 3} \\ U_{\tau 1} & U_{\tau 2} & U_{\tau 3} \end{pmatrix}.$$

This general case requires a great deal of experimental information to pin down, but we can make inferences about specific models. Including solar neutrino results suggests a model where two of the neutrino masses are very close together, and the third is larger:

$$m_3 = M > m = m_1 = m_2,$$

with SuperK's $\Delta m^2 = M^2 - m^2$. In this problem, assume this mass spectrum and also assume that there is no *CP* violation.

(a) What does the assumption of no *CP* violation tell us about the matrix *U*?

(b) Derive the probability of $\nu_\mu \to \nu_\tau$ as a function of distance from the source. (*Hint*: It helps to put in the mass model early in the calculation.)

(c) When interpreted as two-generation mixing, SuperK measures $\sin^2(2\theta) \approx 1$. In our model of three-generation mixing, what is this a measurement of? To allow a definite result, assume that SuperK measures $\sin^2(2\theta) = 0.98$ and that $U_{\tau 3} = 1/\sqrt{2}$. What is the amplitude of ν_μ oscillations to electron neutrinos?

2. MSW effect. Just as with light, the propagation of neutrinos through a material medium can be characterized by an index of refraction. This neutrino index of refraction plays an important role in the MSW hypothesis concerning the shortage of electron-type neutrinos coming from the sun. As with light, the index of refraction n can be related to the neutrino energy $\hbar\omega$, the number density N of scatters in the medium, and the scattering amplitude f for *forward* neutrino scattering:

$$n = 1 + \frac{2\pi N}{k^2} f$$

where $k = \omega/c$.

(a) According to the Standard Model, electron-type and muon-type neutrinos are expected to have different scattering amplitudes, hence different indices of refraction. Explain qualitatively why this is so, referring to appropriate Feynman diagrams as necessary. (This difference is at the heart of the MSW mechanism.)

(b) We are concerned here with neutrino energies small compared to the rest energy of the intermediate vector bosons but large compared to electron binding energies of atoms. Suppose that the medium is composed of neutral atoms of number density N, with Z electrons and $A - Z$ neutrons per atom. Let G_F be the standard "four-fermion" coupling constant of ordinary β-decay. For the purposes of this question, treat the neutrinos as massless.

Obtain an explicit expression for the difference, $n_e - n_\mu$, of the indices of refraction of electron-type and muon-type neutrinos of energy $\hbar\omega$.

Evaluate this difference numerically for neutrinos of energy 1 MeV in a medium of hydrogen atoms with number density $N = 5 \times 10^{25}$ atoms/cm^3. The Fermi constant is $G_F \approx 1.166 \times 10^{-5}$ GeV^{-2}.

3. **Double-bang τ-neutrino detection.** Recent experimental measurements suggest that high-energy electron neutrinos produced at astronomical distances oscillate to τ neutrinos before reaching Earth. High-energy neutrino observatories seek to measure the flux of τ neutrinos through neutrino interactions with the polar ice cap in the southern hemisphere. A volume of 1 km^3 of ice is instrumented with phototubes to detect Cherenkov light. The following information may be useful: mass of τ lepton $m_\tau = 1.8$ GeV/c^2, mass of muon $m_\mu = 0.1$ GeV/c^2, mass of electron $m_e = 0.5$ MeV/c^2, and the lifetime of a τ lepton $\tau_\tau = 0.3$ ps.

   (a) Sketch and label the tree-level Feynman diagram of a τ neutrino interacting with the ice to produce a charged tau lepton in the final state.

   Assume for the following parts of the problem that the τ lepton carries away 75% of the initial neutrino energy.

   (b) For a τ neutrino with an energy of 10^7 GeV, estimate the distance in ice that the τ lepton will travel before decaying.

   (c) List four of the possible decay modes of the τ lepton.

   (d) What is the experimental signature of a 10^7 GeV τ neutrino interacting with the polar ice cap? Make a rough plot of the relative amount (not absolute rates) of Cherenkov light seen at a phototube as a function of time. Label in the plot the effect from the τ decay length.

   (e) Several events are observed in the ice that have a single high-energy shower with energies very close to 6.4×10^6 GeV. What flavor of neutrino is responsible for this, and is it the particle or antiparticle which is interacting? Describe what the interaction is and why 6.4×10^6 GeV is special for this detector.

4. **β-Beams.** Design an Earth-based experiment that utilizes ν_e neutrinos from the β-decay of an energetic beam of ^{13}N ions to detect muon appearance. Assume the ^{13}N ion beam circulates in a beamline consisting of two long, straight sections, one pointing toward the center of Earth and the other pointing up toward the sky. A near detector, as shown in figure 6.11, is located just on top of the accelerator, and a far detector is located on the other side of the planet. The energy of the ν_e from the decay $^{13}\mathrm{N} \rightarrow {}^{13}\mathrm{C} e^+ \nu_e$ in the rest frame of the ^{13}N ion is 2.22 MeV.

   (a) What is the minimum energy of the ν_e in the lab frame that is kinematically required to produce an upward-going μ^- from a weak charged-current interaction with a neutron in a target nucleus in the far detector, assuming that $\nu_e \rightarrow \nu_\mu$ oscillations occur on this length scale? What is the corresponding required beam momentum of the ^{13}N ions in the straight section of the accelerator, also known as a *β-beam*?

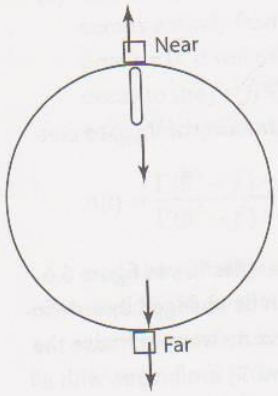

FIGURE 6.11. Vertical ^{13}N ion β-beam with a near detector located above the accelerator and a far detector on the opposite side of the Earth (*not drawn to scale*).

(b) Using the minimum ν_e energy for muon production, the diameter of Earth, and the MNS matrix parameters, what is the probability that the β-decay electron neutrinos have oscillated to muon neutrinos $\nu_e \to \nu_\mu$ by the time they reach the far detector?

(c) If Earth was of sufficiently high density, would it be possible for this experiment to observe matter oscillation enhancement of the mixing? If so, would this effect determine the sign of Δm^2_{31}? Explain.

(d) For an actual experiment, what would be the function of the near detector?

5. **Momentum uncertainty in antineutrinos from a nuclear reactor.** The KamLAND experiment measured neutrino oscillations in antineutrinos coming from nuclear reactors. Show that the momentum uncertainty of antineutrinos coming from free neutron β-decay is compatible with the squared mass difference in antineutrino mass eigenstates from the oscillation signal. Repeat the same analysis for the β-decay of ^{93}Br with a half-life of $T_{1/2} = 102$ ms and for each of the β-decays in the following chain of unstable of fission fragments:

$$^{93}\text{Br} \to {}^{93}\text{Kr} \to {}^{93}\text{Rb} \to {}^{93}\text{Sr} \to {}^{93}\text{Y} \to {}^{93}\text{Kr} \to {}^{93}\text{Nb}. \tag{6.61}$$

6. **Phases of elements of V_{CKM}.** In the Standard Model, the charged-current interactions of the quarks take the form

$$\mathcal{L}_{CC} = -\frac{g}{\sqrt{2}}\left(\bar{u}_L \quad \bar{c}_L \quad \bar{t}_L\right)\gamma^\mu V_{CKM}\begin{pmatrix} d_L \\ s_L \\ b_L \end{pmatrix} W^+_\mu + h.c.,$$

where the W_μ fields correspond to the W bosons and V_{CKM} is a unitary matrix giving the amplitudes for weak transitions between the different flavors of quark. A more explicit representation of V_{CKM} is

$$V_{CKM} = \begin{pmatrix} V_{ud} & V_{us} & V_{ub} \\ V_{cd} & V_{cs} & V_{cb} \\ V_{td} & V_{ts} & V_{tb} \end{pmatrix},$$

where the V_{ab} are complex numbers subject, by virtue of the unitarity of V_{CKM}, to constraints such as

$$V_{cd}V_{cb}^* + V_{td}V_{tb}^* + V_{ud}V_{ub}^* = 0.$$

This constraint can be graphically summarized in "unitary triangles" as in figure 6.6. The phases of the V_{ab} are not individually meaningful: they can be changed by redefining the phases of the quark fields (viz. $u \to \exp(i\alpha)u$). If there is no way to choose the phases of the quarks such that all the V_{ab} are real, then CP (and T) are broken with all the consequences that follow. We will now explore some methods for determining the phases of elements of V_{CKM}.

(a) Consider the neutral mesons $B^0 = \bar{b}d$ and $\bar{B}^0 = b\bar{d}$. The states $|B^0\rangle$ and $|\bar{B}^0\rangle$ are not mass eigenstates because they mix through the diagrams in figure 6.7. To a good approximation (this has to do with the GIM mechanism), these diagrams are dominated by those in which the internal lines are all top quarks. Show that both diagrams are proportional to $(V_{td}V_{tb}^*)^2$. Assuming that all other contributions to the amplitude are real, the overall phase is determined by this CKM factor.

(b) Neither B^0 nor $\bar{B}^0$ are mass eigenstates. To find the mass eigenstates, we must diagonalize a 2×2 Hamiltonian whose off-diagonal elements are given by the mixing amplitude. Show that the energy eigenstates are of the form

$$|B_\pm\rangle = \frac{1}{\sqrt{2}}\left(\exp(i\phi_M)|B^0\rangle \pm \exp(-i\phi_M)|\bar{B}^0\rangle\right)$$

and show that ϕ_M is related to the phase of the $V_{td}V_{tb}^*$ leg of the unitary triangle in figure 6.6.

(c) We observe mixing by watching decays to a channel open to both B^0 and $\bar{B}^0$, such as $B^0(\bar{B}^0) \to J/\Psi\pi^0$, which we assume to proceed via the quark diagrams (we are simplifying reality here) in figure 6.12. Identify the CKM factors associated with these diagrams and show that they correspond to another leg of the unitarity triangle, shown in figure 6.6.

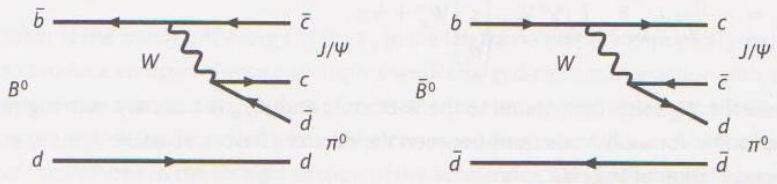

FIGURE 6.12. Decays of the B^0 and $\bar{B}^0$ mesons to the same CP eigenstate.

(d) In what follows we will assume that the complex phase ϕ_W of the decay amplitude comes entirely from the CKM factor. Now suppose that a B^0 (or $\bar{B}^0$) is created at time $t = 0$. It will evolve into a linear combination of B^0 and $\bar{B}^0$ and the rate for decay to the $f = J/\Psi\pi^0$ final state at later times t will have time-dependent interference effects. Construct the time-dependent asymmetry

$$A(t) = \frac{\Gamma(\bar{B}^0 \to f) - \Gamma(B^0 \to f)}{\Gamma(\bar{B}^0 \to f) + \Gamma(B^0 \to f)}$$

and show that by measuring it, one can determine a combination of the phases ϕ_W and ϕ_M. Show that this combined phase is physically meaningful, i.e., is independent of redefinitions of the phases of the quark fields. To what angle of the unitarity triangle does it correspond?

7. Give an example of mixing and decay in the $B_s^0 - \bar{B}_s^0$ system that measures the angle γ in the unitarity triangle.

8. **D^0–$\bar{D}^0$ Mixing**. An abundant source of $D^{*\pm}$ production is from B-hadron decays at B-factories. The flavor of a neutral D meson ($D^0/\bar{D}^0$) coming from $D^{*\pm}$ decay can be tagged by the charge of the soft pion. Assume that the mass difference of the heavy and light neutral D mesons is negligible compared to the average width, i.e., $x = \Delta m/\Gamma \approx 0$. Let the difference in width between the heavy and light neutral D mesons, compared to twice their average width, be given by $y = \Delta\Gamma/(2\Gamma) \approx 1\%$.

   (a) Show that the decay $D^0 \to K^-\pi^+$ is Cabbibo-favored (CF) while the decay $D^0 \to K^+\pi^-$ is doubly Cabbibo suppressed (DCS).

   (b) If the D^0 meson is produced with a momentum of $p = 3$ GeV/c from the decay of a $D^{*\pm}$, what is the typical decay length of the D^0 meson in the lab frame?

   (c) Assume that the $D^0 \to K^+\pi^-$ decay only proceeds through D^0–$\bar{D}^0$ mixing followed by the CF decay $\bar{D}^0 \to K^+\pi^-$. What is the time dependence of the decay rate for small times (i.e., small decay distances in the lab frame)?

   (d) Assume the direct DCS decay $D^0 \to K^+\pi^-$ is two orders of magnitude larger than the probability for D^0–$\bar{D}^0$ mixing followed by the CF decay $\bar{D}^0 \to K^+\pi^-$ in the characteristic time scale of the neutral D-meson lifetime in the lab frame. What is the approximate magnitude of the deviation of the observed $D^0 \to K^+\pi^-$ decay rate from a pure DCS decay rate and how does it depend on time (i.e., decay distance in the lab frame) for small times?

6.7 References and Further Reading

Further information on neutrinos and astroparticle physics can be found here: [6, 7, 8, 9, 10].

A selection of Web sites of related neutrino experiments can be found here: [11, 12, 13, 14, 15, 16, 17, 18, 19, 20].

A selection of Web sites of ultra-high-energy cosmic ray observatories can be found here: [21, 22, 23, 24, 25].

A selection of Web sites of related B-factory experiments can be found here: [26, 27, 28, 29].

Compilations of CKM results can be found here: [5].

[1] Super-Kamiokande Collaboration, *Phys. Rev. Lett.* **81** (1998) 1562.

[2] K. Nakamura et al. (Particle Data Group). *J. Phys. G* **37**, 2010. http://pdg.lbl.gov.

[3] KamLAND Experiment. http://www.awa.tohoku.ac.jp/awa/eng/index.html.

[4] Bahcall, Serenelli, and Basu, *ApJ* **621**, L85 (2005).

[5] CKMfitter. http://ckmfitter.in2p3.fr.

[6] Paul Langacker. *The Standard Model and Beyond*. CRC Press, 2010. ISBN 978-1-4200-7906-7.

[7] Abraham Seiden. *Particle Physics*. Addison-Wesley, 2005. ISBN 0-8053-8736-6.

[8] Rabindra N. Mohapatra and Palash B. Pal. *Massive Neutrinos in Physics and Astrophysics*. World Scientific Publishing, 2004. ISBN 981-238-071-X.

[9] K. Grotz and H. V. Klapdor. *The Weak Interaction in Nuclear, Particle and Astrophysics*. IOP Publishing, 1990. ISBN 0-85274-313-0.

[10] P. D. B. Collins, A. D. Martin, and E. J. Squires. *Particle Physics and Cosmology*. Wiley, 1989. ISBN 0-471-60088-1.

[11] Super-K Experiment on the T2K Beamline. http://www-sk.icrr.u-tokyo.ac.jp/sk/index-e.html.

[12] SNO Experiment, (1999–2006). http://www.sno.phy.queensu.ca.

[13] Borexino Experiment. http://borex.lngs.infn.it.

[14] OPERA Experiment on the CNGS Beamline. http://operaweb.lngs.infn.it.

[15] ICARUS Experiment on the CNGS Beamline. http://icarus.lngs.infn.it.

[16] MINOS Experiment on the NUMI Beamline. http://www-numi.fnal.gov.

[17] NOvA Experiment on the NUMI Beamline. http://www-nova.fnal.gov.

[18] K2K Experiment. http://neutrino.kek.jp.

[19] T2K Experiment. http://jnusrv01.kek.jp/public/t2k/index.html.

[20] Daya Bay Experiment. http://dayawane.ihep.ac.cn.

[21] IceCube Experiment. http://icecube.wisc.edu.

[22] ANTARES Experiment. http://antares.in2p3.fr.

[23] Pierre Auger Observatory. http://www.auger.org.

[24] AGASA at the Akeno Observatory. http://www-akeno.icrr.u-tokyo.ac.jp/AGASA.

[25] HiRes Experiment. http://www.cosmic-ray.org.

[26] CLEO Experiment at CESR. http://www.lns.cornell.edu/public/CLEO.

[27] BaBar Experiment at PEP-II (1999–2008). http://www.public.slac.stanford.edu/babar.

[28] Belle Experiment at KEKB (1999–2010). http://belle.kek.jp.

[29] LHCb Experiment at the LHC. http://lhcb-public.web.cern.ch/lhcb.